

SALIENT SKIN LESION SEGMENTATION VIA DILATED SCALE-WISE FEATURE FUSION NETWORK

Pourya Shamsolmoali * , Masoumeh Zareapoor

Shanghai Jiao Tong University
Shanghai, China

Eric Granger

École de technologie supérieure, Université du Québec
Montreal, Canada

Huiyu Zhou

University of Leicester
Leicester, UK

ABSTRACT

Skin lesion detection in dermoscopic images is essential in the accurate and early diagnosis of skin cancer by a computerized apparatus. Current skin lesion segmentation approaches show poor performance in challenging circumstances such as indistinct lesion boundaries, low contrast between the lesion and the surrounding area, or heterogeneous background that causes over/under segmentation of the skin lesion. To accurately recognize the lesion from the neighboring regions, we propose a dilated scale-wise feature fusion network based on convolution factorization. Our network is designed to simultaneously extract features at different scales which are systematically fused for better detection. The proposed model has satisfactory accuracy and efficiency. Various experiments for lesion segmentation are performed along with comparisons with the state-of-the-art models. Our proposed model consistently showcases state-of-the-art results.

1 INTRODUCTION

Skin melanoma cases represent about 1% of skin cancers but cause most of the skin cancer deaths. According to available data, 192,310 new melanoma cases, 95,830 non-invasive and 96,480 invasive, were reported in the United States between 2019-2020, resulting in around 10,000 deaths¹. To automatically detect melanoma in dermoscopy images, it is imperative to precisely outline the boundary of the lesion in order to carry out proper analysis of the clinical indicators presented in the lesion (Garcia-Arroyo & Garcia-Zapirain, 2019). There are various challenges with effective skin lesion detection in dermoscopy images including variations of lesion size, unclear boundaries, lesion types and different skin colors. Complex background regions (for instance, heterogeneous background (Barata et al., 2018)) in dermoscopic images also make it challenging to recognize the lesions and distinguish them from neighbouring areas. For example, specular reflections and hair are other barriers that reduce the accuracy of the segmentation. Indeed, significant efforts have been carried out in recent years and achieved good progress in this field (Barata et al., 2018). In (Celebi et al., 2015), the authors presented a comprehensive review on detection of lesion border in dermoscopy images.

Salient Object Detection (SOD), as a useful method, can pinpoint the location and outline of the most salient regions or objects in an image. SOD can significantly increase the performance of different computer vision tasks, like object detection (Song et al., 2018; Wang et al., 2019) and segmentation (Mehta et al., 2018). Currently, convolutional neural networks (CNNs) models have emerged as a promising support for SOD and regularly reported major improvements (Song et al., 2018; Wang et al., 2019; Mehta et al., 2018). Despite this progress, how to devise an efficient yet effective CNN model for SOD remains an open challenge. To address the above problem, we pro-

*pshams55@gmail.com

¹<https://www.aad.org/media/stats-skin-cancer>

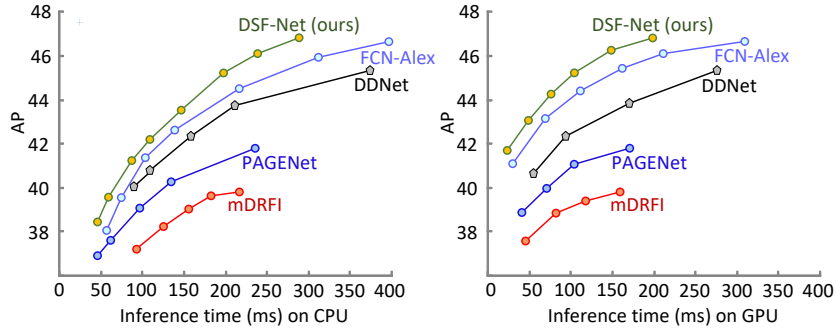


Figure 1: Average Precision (AP) vs. inference time per image. The green curve shows results of DSF-Net which is described in the text body.

pose a *dilated scale-wise feature fusion (DSF)* for skin lesion segmentation, to significantly reduce the computational complexity of CNNs (Mehta et al., 2018; Xie et al., 2017; Szegedy et al., 2017). Based on the DSF units, we introduce a network called, DSF-Net, that can be used for semantic segmentation. DSF-Net has achieved satisfactory segmentation accuracy with minor latency.

Fig. 1 shows a summary of comparison results. DSF decomposes a typical convolution operation into two stages: instant convolutions and dilated pyramid convolutions, as shown in Fig. 2. To reduce the memory usage of our proposed model while training, we do not use data augmentation. However, to increase the robustness, we use an instant convolution, where the weight matrix is initialized as a random rotation matrix (Dohmatob & Bietti, 2022). This simple method improves the generalization and robustness to domain distribution. The instant convolutions are also effective in reducing the computational cost, whereas the dilated pyramid networks re-sample the feature maps in order to widely learn from a large and more useful receptive field. In addition, scale-wise feature fusion is adopted to aggregate different scale features. We show that the proposed DSF model has better segmentation accuracy and efficiency compared to other factorized convolution models. It has been observed that the existing pyramid models (Song et al., 2018; Wang et al., 2019; Mehta et al., 2018) have high computational costs and cannot be applied at different CNN layers and at any spatial level for representation learning. In contrast to the above mentioned methods, DSF unit has lower computation costs, therefore, can be efficiently applied at any spatial layer of a CNN. Current dilated convolution models (Song et al., 2018; Shamsolmoali et al., 2019b,a) are inefficient, but our proposed DSF model utilizes an efficient dilated convolutions. To evaluate the performance of DSF-Net, comprehensive experiments on four publicly accessible datasets have been conducted. DSF-Net demonstrates to be more accurate and efficient than the other state-of-the-art.

2 RELATED WORK

Accurate segmentation of the lesion from the normal skin is useful for effective skin cancer diagnosis (Ünver & Ayan, 2019). The segmentation methods are categorised to three groups. Histogram thresholding models apply a threshold value for the lesion segmentation (Garcia-Arroyo & Garcia-Zapirain, 2019; Unnikrishnan et al., 2007). Unsupervised models, unlike the supervised approaches, do not need any training. They utilize different image processing approaches to enhance the colour, and spatial location which have a significant impact on visual attention (Ahn et al., 2017). The last one is the supervised segmentation models. Such approaches segment the skin lesions by training a detection network such as SVM and artificial neural networks (Xie & Bovik, 2013). But, these traditional methods cannot achieve satisfactory segmentation results and unable to overcome the problems like unclear lesion boundaries, and hair. Recently, CNNs have achieved a great progress in detection, and segmentation of objects (Wang et al., 2019; Mehta et al., 2018; Xie et al., 2017).

In (Kaymak et al., 2020), a model based fully convolution network (FCN) is proposed for skin lesion segmentation. In the implementation, a new FCN architecture is designed based on the AlexNet (Krizhevsky et al., 2012) called FCN-AlexNet. A variational autoencoder is used to label skin tone of lesion images (Bevan & Atapour-Abarghouei, 2022) and this framework is used to

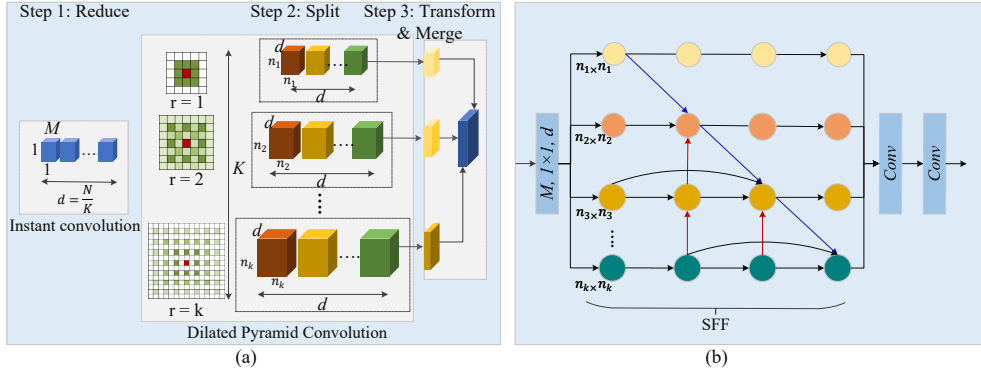


Figure 2: Diagram of the proposed DSF model: (a) the DSF unit is decomposed into instant convolution and dilated pyramid convolutions; (b) Block diagram of pyramid unit.

annotate the benchmark datasets for lesion detection. This is a useful method for data annotation, nevertheless, this model does not perform effectively for complex images. In (Liu et al., 2021) a CNN architecture based on auxiliary information is proposed, where edge prediction is conducted as an auxiliary task alongside the segmentation task. Furthermore, a multi-scale feature aggregation module is suggested, which utilizes features of several scales. These models, however, perceive dark regions to be regions of interest, and their segmentation performance is low when the region of interest is brighter than the surrounding skin region. (Sarker et al., 2021) proposes a lightweight generative adversarial network that integrates 1-D kernel weighted networks, position, and channel attention. The position and channel attention modules, respectively, improve the discriminative ability between lesion and non-lesion feature representations in spatial and channel dimensions. In (Akyel & Arici, 2022; Kosgiker et al., 2022), CNNs based methods are introduced for noise reduction and lesion segmentation. Noise reduction such as hair removal is important for a correct segmentation of the lesions. However, these models require complex parameter adjustment that increases the computation cost. The key reason for the success of CNNs is due to their ability in extracting deep and robust features from the input images and their hierarchical feature learning. Several approaches such as network compression and factorized convolutional kernels have been introduced to accelerate CNNs (Mehta et al., 2018; Szegedy et al., 2017).

Convolution factorization is an effective approach which breaks down the convolutional operation into multiple stages to ensure a fast computation. Factorization has demonstrated its ability in dropping the computational complexity for deep CNNs such as Inception (Szegedy et al., 2017), and factorized network (Jin et al., 2014).

Dilated convolution (Shamsolmoali et al., 2019b,a) is a type of conventional convolution in which the effective receptive field of the kernel is enlarged by adding zeros between each pixel in the convolutional kernel. As an example, for $n \times n$ dilated convolution kernel, the operative size of the kernel is $[(n-1)r+1]^2$.

3 PROPOSED DILATED SCALE-WISE FEATURE FUSION NETWORK

As shown in Fig. 2(a), the proposed DSF-Net is composed of an instant convolution and dilated pyramid convolutions. A 1×1 instant convolution is used to increase the robustness and reduce the dimension of feature maps. Then, the dilated pyramid convolutions resample the rescaled feature maps with $n \times n$ dilated convolutional K kernels, in which the dilation rate is $2^{(k-1)}$ where $k = 1, 2, \dots, k$. In our model the factorization technique considerably decreases the memory usage and the number of parameters, while keeping the potential receptive fields $[(n-1)^{2^{k-1}} + 1]^2$. In the proposed DSF unit, each kernel of the dilated convolution uses multiple receptive fields for weights learning. A typical convolution layer receives an input $F_i \in R^{H \times W \times M}$ and has N kernels $K \in R^{m \times n \times M}$ for generating a feature map $F_0 \in R^{(H \times W \times N)}$, in which

H, W indicate the feature map dimension, while m, n are the dimension of the kernel (width and height), and M, N are the total input and output feature channels. For better understanding, we assume $m = n$. The ordinary convolution kernels learn $(n^2 MN)$ parameters. Indeed, these parameters are based on the kernels dimension, the number of input M and output N channels.

Width splitting and Network Design: To increase the efficiency of the proposed DSF unit, the hyperparameter K is introduced. K participates to split the dimension of the feature maps consistently through each DSF unit. For a certain K , the DSF unit in the first step decreases the feature maps from M dimensions to $\frac{N}{K}$ dimensions as shown in Fig. 2(a). Then, the feature maps shrink between K branches that have different scales. In each branch of the saliency network, a pyramid attention module is placed which is integrated to generate high discriminative feature maps. Different from current saliency models that consider all the points equally in a saliency feature map, DSF only focuses on the important regions features and reuses the multi-scale information by several attention layers which take advantage of scale-wise features to build a uniform pyramid network. To be more precise, let X represent a feature map extracted from a convolution layer of a saliency network with C channels, $X \in R^{M \times N \times C}$. We aim to learn a group of same size attention masks that the weight of saliency features X are built on scale-wise information. Multi-scale features are obtained by stepwise down-sampling of X for generating low resolution feature maps $X^n \in R^{\frac{M}{2^n} \times \frac{N}{2^n} \times C}$; ($n = 1, 2, 3, \dots, N$), for $i \in 1, \dots, \frac{M}{2^n} \times \frac{N}{2^n}$.

$$\ell_i^n = p(L = i | X^n) = \frac{\exp(W_i^n \times X_i^n)}{\sum_{j=1}^{\frac{M}{2^n} \times \frac{N}{2^n}} \exp(W_j^n \times X_i^n)} \quad (1)$$

in which W_i^n denotes the weights of the hidden layer, $j = 1$ is a constant value, L represents a random variable; ℓ is the attention map, where $\sum_i^{\frac{M}{2^n} \times \frac{N}{2^n}} \ell_i = 1$. With these operations, DSF learns from attention maps of different regions at different scales. This is required for saliency segmentation as salient areas need higher weights. Moreover, stacked pooling is applied in pyramid units to improve the receptive field of different feature extraction layer, and feature representation can be enhanced by merging the features of different regions

$$\begin{aligned} \Upsilon_j &= \underbrace{\frac{1}{N} \sum_{n=1}^N \ell_j^n X_j}_{(j \in 1, \dots, (M \times N))} \\ &= \underbrace{\frac{1}{N} \sum_{n=1}^N (1 + \ell_j^n) X_j}_{\text{term (a)}}_{(j \in 1, \dots, (M \times N))} \\ &\quad \underbrace{\quad}_{\text{term (b)}} \end{aligned} \quad (2)$$

in which Υ denotes the updated feature and Υ_j represents the j^{th} feature map. As illustrated in Eq. 2 term (a), the model estimates the engaged parameters for the inputs by targeting the expectation over the image features in various areas. To reduce the number of null values in the feature maps and simplify the back-propagation we adopt identity mapping (He et al., 2016) as presented in Eq. 2 term (b). By adopting the residual connection we can preserve the input features. The outputs of the K parallel dilated convolution are merged to generate *multi-dimensional* feature map, Fig. 2(b) represents our approach. Our DSF module has $\frac{MN}{K} + \frac{(nN)^2}{K}$ parameters and the size of its receptive field is $[(n-1)2^{(k-1)} + 1]^2$. In comparison with the ordinary convolution layers, factorization significantly moderates the number of parameters by a factor of $\frac{n^2 MK}{M+n^2 N}$. Thus, the DSF unit learns $\sim 2.5 \times$ fewer parameters with a receptive field of 15×15 than an ordinary convolution with a 3×3 receptive field, where $K = 4$, and $N = M = 128$.

Feature Pyramid Module: X represents the feature from the last convolution layers of the DSF units. Each X^ℓ is firstly downsampled into various scales. The network attention is calculated over three sequential operations: Batch Normalization (BN) is followed by $(1 \times 1, 1)$ convolution and ReLU, with the 14×14 attention maps. To resize the attention maps $(\ell^n)_n$ to its original size, upsampling is applied over all the scales to achieve an enhanced saliency representation X^ℓ via Eq.(2). To enhance the semantic of features in each level of the pyramid network, a weighting

module is applied. Assume F_n are the feature maps in n^{th} pyramid level. If H_n and W_n represent the height and width of F_n , respectively, and F_n^i denotes the i^{th} channel feature. We compute the global distribution response Z_n^i by using global average pooling on F_n^i , as follows:

$$Z_n^i = \frac{1}{H_n \times W_n} \sum_p \sum_q F_n^i(f, q) \quad (3)$$

In order to compute the weight, two 1×1 convolution layers are used to map the non-linear correlation among distribution responses Z_n and acquire the significant feature vectors $\hat{Z}_n = W_n^1(\delta(W_n^2 Z_n))$, in which W_n^1 and W_n^2 are the weights of the first and the second convolution layers respectively and δ signifies the activation function. We use Sigmoid σ to normalize \hat{Z}_n as a weight vector $r_n = \sigma(\hat{Z}_n)$, and obtained the channel-wised feature weight F_{cr_n} , as follows:

$$F_{cr_n} = F_n r_n = [F_n^1 r_n^1, F_n^2 r_n^2, \dots, F_n^n r_n^n] \quad (4)$$

Moreover, to improve the features, we define a function $F_n^{(f,q)}$ to unify the channel features at each point (f, q) on F_n (Zhou et al., 2021). Firstly, the pointwise addition is performed on channel features to obtain the spatial vector $V_n^{(f,q)}$ while W_n^3 denotes the kernel weight of the convolution layer as: $V_n^{(f,q)} = W_n^3 F_n^{(f,q)}$. To generate the weight t_n , we normalize the spatial vector V_n as $t_n = \sigma(V_n)$, therefore, the new spatial feature weight F_{sr_n} is written as:

$$F_{sr_n} = F_n t_n = [F_n^{(1,1)} t_n^{(1,1)}, F_n^{(1,2)} t_n^{(1,2)}, \dots, F_n^{(H_n, W_n)} t_n^{(H_n, W_n)}] \quad (5)$$

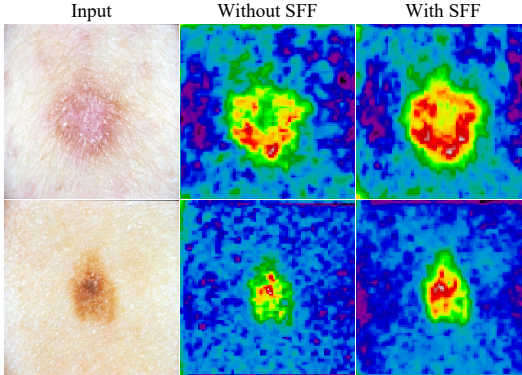


Figure 3: Comparison of DSF module feature maps *with* & *without* stepwise feature fusion (SFF). SFF rectifies the gridding artifact.

Finally, we combine the channel-wised feature weight F_{cr_n} , and the spatial feature weight F_{sr_n} to make an enhanced feature $F_{rn} = F_{cr_n} + F_{sr_n}$ to capture more important information.

Stepwise Feature Fusion (SFF): By combining the results of the dilated convolutions, the proposed DSF unit provides a large receptive field. However, it generates some undesirable artifacts, as shown in Fig. 3. To get rid of these artifacts, we propose to merge the obtained feature maps from different kernel scales and dilation rates before concatenating them, as shown in Fig. 2 that helps to pay more attention to the global information and further refines the focus area of the model. This effective and simple solution will not increase the network complexity. The network only uses an element-wise addition to combine the input and output feature maps (He et al., 2016).

DSF-Net architecture: Except the first layer where standard convolution is used, in the rest of proposed network, DSF modules are adopted for learning and down-sampling tasks. All the convolution layers and the DSF units are followed by *BN* (Ioffe & Szegedy, 2015) and *ReLU* (He et al., 2015). Then the output features are processed by a 1×1 convolution and sigmoid for generating the saliency map. To upscale the saliency map into its original size we use bilinear interpolation. Fig. 4 in detail illustrates the architecture of DSF-Net. The saliency segmentation outputs have the same size as that of the input image and a light weight decoder is used. A hyperparameter α controls the depth of the network to create a deep efficient network while preserving the network topology. Generally CNNs demanding additional memory at higher spatial levels due to the high dimensions of feature maps. However, neither the convolution layer nor the DSF units are repeated at these stages.

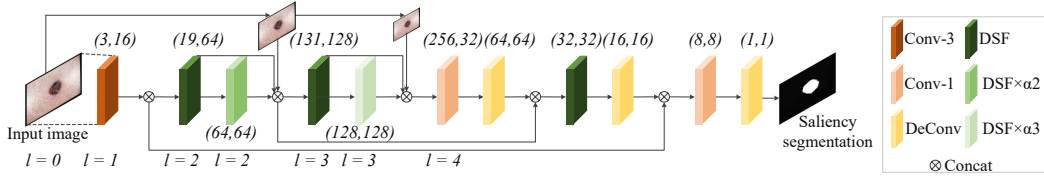


Figure 4: The architecture of *DSF-Net*. The *Conv* – 3 and *DSF* modules perform down-sampling and *DeConv* module performs up-sampling actions. For each layer the *input channels* and *output channels* are shown.

Loss Function: To improve saliency prediction and training, a fused loss function is proposed on the basis of various evaluation metrics. Let $G \in [0, 1]_{r \times q}$ and $S \in [0, 1]_{r \times q}$ be the input saliency map and the estimated saliency respectively, in which $r \times q$ denotes the resolution of the saliency map, and the final loss \mathcal{L} computed as:

$$\mathcal{L}(G, S) = \mathcal{L}_{Crossentropy}(G, S) + \mathcal{L}_{MAE}(G, S) \quad (6)$$

in which $\mathcal{L}_{crossentropy}$ and \mathcal{L}_{MAE} specify *cross entropy* and *MAE loss* respectively. \mathcal{L}_{MAE} is based on the *MAE* metric, which is widely used in the identification of salient objects. \mathcal{L}_{MAE} calculates the variance between the predicted saliency map S and the corresponding ground truth G .

Table 1: Quantitative evaluation with F_{score} and RPI (higher is better), MAE (lower is better) over four skin lesions datasets. For each column, the best result is highlighted.

Methods	ISBI-2016			ISBI-2017			PH2			ISIC-2018		
	F_{score}	MAE	PRI									
mDRFI	0.729	0.056	0.732	0.714	0.058	0.739	0.691	0.052	0.708	0.721	0.051	0.737
eVida	0.742	0.059	0.757	0.726	0.059	0.733	0.705	0.054	0.712	0.737	0.053	0.748
YGC	0.816	0.051	0.825	0.803	0.054	0.818	0.759	0.043	0.766	0.821	0.052	0.819
DDNet	0.878	0.043	0.889	0.863	0.043	0.874	0.843	0.034	0.851	0.869	0.045	0.876
PAGENet	0.786	0.048	0.795	0.769	0.048	0.772	0.752	0.032	0.760	0.775	0.047	0.781
SRM	0.731	0.044	0.739	0.698	0.047	0.706	0.679	0.039	0.685	0.713	0.046	0.722
FCN-AlexNet	0.904	0.041	0.916	0.889	0.044	0.895	0.872	0.034	0.879	0.895	0.043	0.903
DSF w/o SFF	0.856	0.053	0.862	0.838	0.049	0.845	0.819	0.037	0.827	0.842	0.054	0.851
DSF-Net	0.908	0.040	0.919	0.894	0.046	0.901	0.876	0.033	0.882	0.897	0.042	0.901

Table 2: Quantitative evaluation with VOI, GCE and BDE (for all metrics lower is better) over four skin lesions datasets. For each column, the best result is highlighted.

Methods	ISBI-2016			ISBI-2017			PH2			ISIC-2018		
	VOI	GCE	BDE	VOI	GCE	BDE	VOI	GCE	BDE	VOI	GCE	BDE
mDRFI	1.593	0.167	16.07	1.684	0.173	17.26	1.698	0.194	17.41	1.664	0.169	16.57
eVida	1.579	0.164	14.32	1.673	0.169	15.52	1.683	0.181	15.69	1.662	0.166	15.46
YGC	1.574	0.155	12.37	1.663	0.166	13.06	1.678	0.186	13.22	1.582	0.159	12.48
DDNet	1.567	0.154	9.46	1.654	0.148	10.73	1.672	0.166	10.88	1.574	0.160	9.50
PAGENet	1.569	0.155	10.86	1.667	0.162	11.41	1.676	0.179	11.63	1.575	0.156	10.92
SRM	1.565	0.149	9.51	1.654	0.159	10.99	1.669	0.161	10.39	1.569	0.153	9.59
FCN-AlexNet	1.558	0.148	9.43	1.652	0.156	10.38	1.667	0.168	10.59	1.573	0.151	9.52
DSF-Net	1.556	0.149	9.41	1.651	0.152	10.11	1.663	0.163	10.34	1.562	0.152	9.51

4 EXPERIMENTS AND PROTOCOLS

To evaluate the proposed DSF-Net, four datasets have been used ISBI-2016, ISBI-2017, PH2, and ISIC-2018. The ISBI-2016 contains 1,279 dermoscopic images and the ISBI-2017 (Gutman et al., 2016) consists of 23,906 images. PH2 dataset (Mendonça et al., 2013), contains 200 dermoscopic images and ISIC-2018 dataset (Codella et al., 2018) contains 2594 dermoscopic images. For a comprehensive evaluation, we use several metrics: *Precision-Recall* (PR) curves, *F-measure*, *Mean Absolute Error* (MAE), *Variation of Probabilistic Rand Index* (PRI), *Information metric* (VOI), *Global Consistency Error* (GCE), and *Boundary Displacement Error* (BDE) (Shamsolmoali et al., 2020). A segmentation result is satisfactory based on these parameters when the comparison with ground truth gives high values for the *F-measure* and PRI, but low values for the other metrics. Pytorch is used for all the implementations. Based on the training protocol shown in (Ünver & Ayan, 2019), we

used ISBI-2017 for training. The stochastic gradient descent optimizer is used to train our proposed model with a batch size of 16. The learning rate is set to 0.001 and it is decreased by a factor of 0.01 after 100 and 200 epochs. Moreover, we have set the weight decay factor to 0.0005 and the momentum to 0.9. We trained the model for 300 epochs which takes around 4 hours using an Nvidia GTX 1080 GPU. DSF-Net processes an input image in 0.45s which is faster than the current salient segmentation based CNN approaches.

5 RESULTS AND ANALYSIS

We evaluate the performance of DSF-Net against the other recent approaches such as: mDRFI (Jahanifar et al., 2018), eVida (Garcia-Arroyo & Garcia-Zapirain, 2019), YGC (Ünver & Ayan, 2019), DDNet (Li et al., 2018), PAGENet (Wang et al., 2019), SRM (Wang et al., 2017), and FCN-AlexNet (Kaymak et al., 2020).

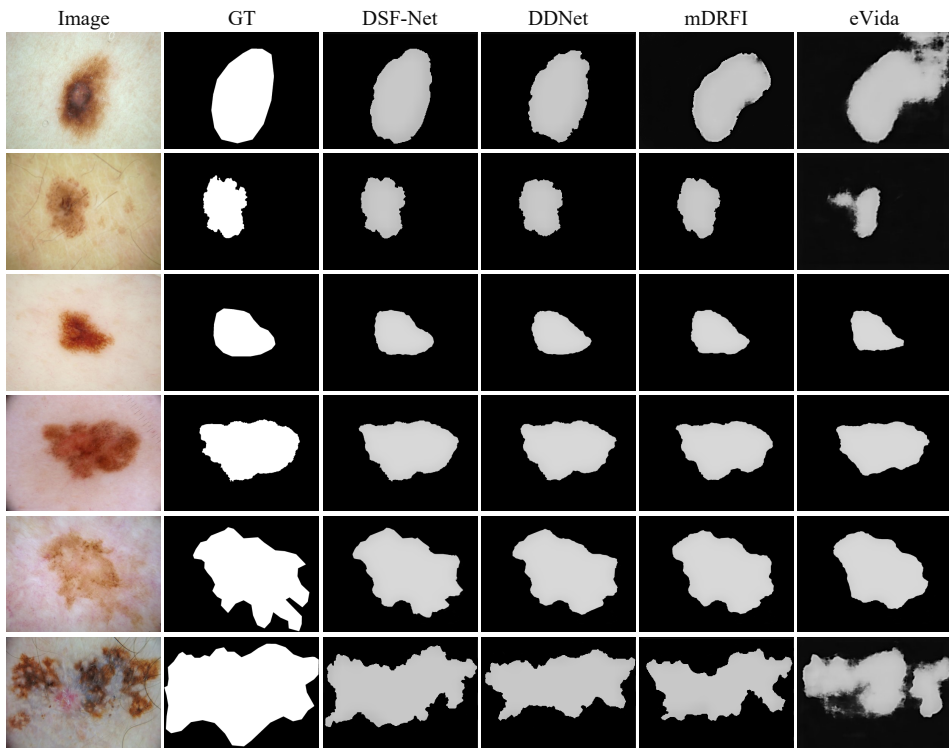


Figure 5: Segmentation and visualize results for different methods on some representative examples.

In Table 3 we report the test results of DSF-Net and the other approaches on all four datasets in terms of F-measure, MAE and PRI scores. DSF-Net considerably improved F-measure compare to the other approaches. Moreover, in Table 3 we report the test results of DSF-Net and the other approaches in terms of VOI, GCE, and BDE scores. The results validates the superior performance of DSF-Net in different scenes. In Fig. 5 we visualize the segmentation results of different models. From this results we observe DSF-Net has better performance in a variety of complex situations, for example, large lesions, while there is low contrast between lesions and the surrounding skin, and multiple disconnected lesions. Furthermore, DSF-Net captures boundaries properly because of using salient edge detection. Here, we evaluate the contribution of each module to the overall performance of the proposed DSF-Net. The experiments conducted on the ISBI-2016 and ISBI-2017.

Down-sampling and Residual learning: Replacing the standard convolution with the strided DSF and skip-connections in the proposed DSF-Net improved accuracy by 3% with 26% parameter reduced. This verifies the effectiveness of the selected learning scheme. The PR curves of all approaches are shown in Fig. 6 on two datasets. We observe that DSF-Net achieved a higher ROC score (4.2% better) comparing to that obtained by other models in the testing set. The fact that

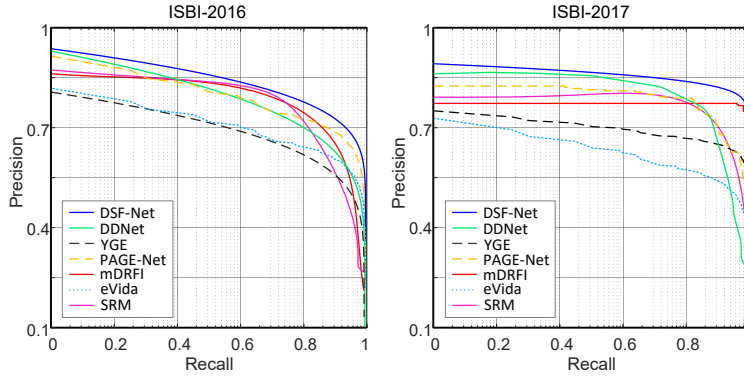


Figure 6: Quantitative comparison of six models using PR curve on ISBI-2016 and ISBI-2017 datasets.

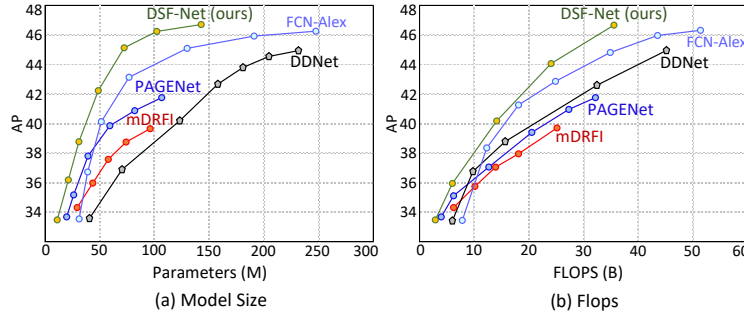


Figure 7: Efficiency comparison of state-of-the-art models.

DSF-Net not only learns highly abstract salient features of skin lesions with a lower number of parameters but also results in improving semantic segmentation and can be used for lesion segmentation.

Effect of different convolutions in the DSF modules: The DSF module uses instant convolutions to rotate and reduce the dimension of feature maps whilst using dilated pyramid convolutions to transform the feature maps. To show the effect of these two components, the following experiments are performed. Instant convolutions: standard convolutions with rotated matrix are substituted with dilated pyramid convolutions in the DSF module; the resultant network is more efficient with a less number of parameters and improves the saliency segmentation by 1.5%. Fig. 7 shows the performance of DSF-Net in comparison with the other state-of-the-art models. DSF modules outperformed mDRFI and PAGENet by 1.14% and 1.08%, respectively, while learning the same number of parameters with lower network sizes and higher speeds. In addition to the parameter size and FLOPs, we have also evaluated the latency of the algorithms. Each model runs 5 times with the batch size 1, the standard deviation and mean are reported. Fig. 7 reveals the performance on the model size, flops and GPU latency. In comparison with the other state-of-the-art models, DSF-Net can make 1.6 \times faster when using GPU. Overall, DSF-Net shows satisfactory segmentation performance with better boundary adherence and less displacement errors in these experiments.

6 CONCLUSION

We have introduced a novel saliency segmentation model, DSF-Net, based on an efficient dilated pyramid network. The proposed model improves feature extraction and saliency representations with stepwise dilated convolution. In addition, instant convolution enables more efficient training and better performance. Extensive experimental evaluations on three benchmark datasets demonstrate that our algorithm significantly improved segmentation performance. In addition, the proposed DSF-Net architecture has better efficiency when using GPUs for acceleration.

REFERENCES

Euijoon Ahn, Jinman Kim, Lei Bi, Ashnil Kumar, Changyang Li, Michael Fulham, and David Dagan Feng. Saliency-based lesion segmentation via background detection in dermoscopic images. *IEEE journal of biomedical and health informatics*, 21(6):1685–1693, 2017.

Cihan Akyel and Nursal Arıcı. Linknet-b7: Noise removal and lesion segmentation in images of skin cancer. *Mathematics*, 10(5):736, 2022.

Catarina Barata, M Emre Celebi, and Jorge S Marques. A survey of feature extraction in dermoscopy image analysis of skin cancer. *IEEE journal of biomedical and health informatics*, 23(3):1096–1109, 2018.

Peter J Bevan and Amir Atapour-Abarghouei. Detecting melanoma fairly: Skin tone detection and debiasing for skin lesion classification. *arXiv preprint arXiv:2202.02832*, 2022.

M Emre Celebi, QUAN Wen, HITOSHI Iyatomi, KOUHEI Shimizu, Huiyu Zhou, and Gerald Schaefer. A state-of-the-art survey on lesion border detection in dermoscopy images. *Dermoscopy image analysis*, 10:97–129, 2015.

Noel CF Codella, David Gutman, M Emre Celebi, Brian Helba, Michael A Marchetti, Stephen W Dusza, Aadi Kalloo, Konstantinos Liopyris, Nabin Mishra, Harald Kittler, et al. Skin lesion analysis toward melanoma detection: A challenge at the 2017 international symposium on biomedical imaging (isbi), hosted by the international skin imaging collaboration (isic). In *2018 IEEE 15th International Symposium on Biomedical Imaging*, pp. 168–172. IEEE, 2018.

Elvis Dohmatob and Alberto Bietti. On the (non-) robustness of two-layer neural networks in different learning regimes. *arXiv preprint arXiv:2203.11864*, 2022.

Jose Luis Garcia-Arroyo and Begonya Garcia-Zapirain. Segmentation of skin lesions in dermoscopy images using fuzzy classification of pixels and histogram thresholding. *Computer methods and programs in biomedicine*, 168:11–19, 2019.

David Gutman, Noel CF Codella, Emre Celebi, Brian Helba, Michael Marchetti, Nabin Mishra, and Allan Halpern. Skin lesion analysis toward melanoma detection: A challenge at the international symposium on biomedical imaging (isbi) 2016, hosted by the international skin imaging collaboration (isic). *arXiv preprint arXiv:1605.01397*, 2016.

Kaiming He, Xiangyu Zhang, Shaoqing Ren, and Jian Sun. Delving deep into rectifiers: Surpassing human-level performance on imagenet classification. In *Proceedings of the IEEE international conference on computer vision*, pp. 1026–1034, 2015.

Kaiming He, Xiangyu Zhang, Shaoqing Ren, and Jian Sun. Deep residual learning for image recognition. In *Proceedings of the IEEE conference on computer vision and pattern recognition*, pp. 770–778, 2016.

Sergey Ioffe and Christian Szegedy. Batch normalization: Accelerating deep network training by reducing internal covariate shift. *arXiv preprint arXiv:1502.03167*, 2015.

Mostafa Jahanifar, Neda Zamani Tajeddin, Babak Mohammadzadeh Asl, and Ali Gooya. Supervised saliency map driven segmentation of lesions in dermoscopic images. *IEEE journal of biomedical and health informatics*, 23(2):509–518, 2018.

Jonghoon Jin, Aysegul Dundar, and Eugenio Culurciello. Flattened convolutional neural networks for feedforward acceleration. *arXiv preprint arXiv:1412.5474*, 2014.

Ruya Kaymak, Cagri Kaymak, and Aysegul Ucar. Skin lesion segmentation using fully convolutional networks: A comparative experimental study. *Expert Systems with Applications*, 161: 113742, 2020.

Gouse Mohiuddin Kosgiker, Anupama Deshpande, and Kauser Anjum. Significant of multi-level pre-processing steps and its proper sequence in segcaps skin lesion segmentation of dermoscopic images. *Materials Today: Proceedings*, 51:129–141, 2022.

Alex Krizhevsky, Ilya Sutskever, and Geoffrey E Hinton. Imagenet classification with deep convolutional neural networks. *Advances in neural information processing systems*, 25, 2012.

Hang Li, Xinzi He, Feng Zhou, Zhen Yu, Dong Ni, Siping Chen, Tianfu Wang, and Baiying Lei. Dense deconvolutional network for skin lesion segmentation. *IEEE journal of biomedical and health informatics*, 23(2):527–537, 2018.

Lina Liu, Ying Y Tsui, and Mrinal Mandal. Skin lesion segmentation using deep learning with auxiliary task. *Journal of Imaging*, 7(4):67, 2021.

Sachin Mehta, Mohammad Rastegari, Anat Caspi, Linda Shapiro, and Hannaneh Hajishirzi. Espnet: Efficient spatial pyramid of dilated convolutions for semantic segmentation. In *Proceedings of the european conference on computer vision*, pp. 552–568, 2018.

Teresa Mendonça, Pedro M Ferreira, Jorge S Marques, André RS Marcal, and Jorge Rozeira. Ph 2-a dermoscopic image database for research and benchmarking. In *2013 35th annual international conference of the IEEE engineering in medicine and biology society (EMBC)*, pp. 5437–5440. IEEE, 2013.

Md Mostafa Kamal Sarker, Hatem A Rashwan, Farhan Akram, Vivek Kumar Singh, Syeda Furruka Banu, Forhad UH Chowdhury, Kabir Ahmed Choudhury, Sylvie Chambon, Petia Radeva, Domenec Puig, et al. Slsnet: Skin lesion segmentation using a lightweight generative adversarial network. *Expert Systems with Applications*, 183:115433, 2021.

Pourya Shamsolmoali, Xiaofang Li, and Ruili Wang. Single image resolution enhancement by efficient dilated densely connected residual network. *Signal Processing: Image Communication*, 79:13–23, 2019a.

Pourya Shamsolmoali, Junhao Zhang, Jie Yang, et al. Image super resolution by dilated dense progressive network. *Image and Vision Computing*, 88:9–18, 2019b.

Pourya Shamsolmoali, Masoumeh Zareapoor, Huiyu Zhou, Ruili Wang, and Jie Yang. Road segmentation for remote sensing images using adversarial spatial pyramid networks. *IEEE Transactions on Geoscience and Remote Sensing*, 59(6):4673–4688, 2020.

Hongmei Song, Wenguan Wang, Sanyuan Zhao, Jianbing Shen, and Kin-Man Lam. Pyramid dilated deeper convlstm for video salient object detection. In *Proceedings of the European Conference on Computer Vision*, pp. 715–731, 2018.

Christian Szegedy, Sergey Ioffe, Vincent Vanhoucke, and Alexander A Alemi. Inception-v4, inception-resnet and the impact of residual connections on learning. In *Thirty-first AAAI conference on artificial intelligence*, 2017.

Ranjith Unnikrishnan, Caroline Pantofaru, and Martial Hebert. Toward objective evaluation of image segmentation algorithms. *IEEE transactions on pattern analysis and machine intelligence*, 29(6):929–944, 2007.

Halil Murat Ünver and Enes Ayan. Skin lesion segmentation in dermoscopic images with combination of yolo and grabcut algorithm. *Diagnostics*, 9(3):72, 2019.

Tiantian Wang, Ali Borji, Lihe Zhang, Pingping Zhang, and Huchuan Lu. A stagewise refinement model for detecting salient objects in images. In *Proceedings of the IEEE International Conference on Computer Vision*, pp. 4019–4028, 2017.

Wenguan Wang, Shuyang Zhao, Jianbing Shen, Steven CH Hoi, and Ali Borji. Salient object detection with pyramid attention and salient edges. In *Proceedings of the IEEE Conference on Computer Vision and Pattern Recognition*, pp. 1448–1457, 2019.

Fengying Xie and Alan C Bovik. Automatic segmentation of dermoscopy images using self-generating neural networks seeded by genetic algorithm. *Pattern Recognition*, 46(3):1012–1019, 2013.

Saining Xie, Ross Girshick, Piotr Dollár, Zhuowen Tu, and Kaiming He. Aggregated residual transformations for deep neural networks. In *Proceedings of the IEEE conference on computer vision and pattern recognition*, pp. 1492–1500, 2017.

Bo Zhou, S Kevin Zhou, James S Duncan, and Chi Liu. Limited view tomographic reconstruction using a cascaded residual dense spatial-channel attention network with projection data fidelity layer. *IEEE transactions on medical imaging*, 40(7):1792–1804, 2021.